Open Archive TOULOUSE Archive Ouverte (OATAO)

OATAO is an open access repository that collects the work of Toulouse researchers and makes it freely available over the web where possible.

Any correspondence concerning this service should be sent to the repository administrator: staff-oatao@listes-diff.inp-toulouse.fr

Interaction of graphene-related materials with human intestinal cells: an *in vitro* approach†

M. Kucki,*[a] P. Rupper,[b] C. Sarrieu,[c] M. Melucci,[d] E. Treossi,[d] A. Schwarz,[e] V. León,[f] A. Kraegeloh,[e] E. Flahaut,[c] E. Vázquez,[f] V. Palermo[d] and P. Wick*[a]

Graphene-related materials (GRM) inherit unique combinations of physicochemical properties which offer a high potential for technological as well as biomedical applications. It is not clear which physicochemical properties are the most relevant factors influencing the behavior of GRM in complex biological environments. In this study we have focused on the interaction of GRM, especially graphene oxide (GO), and Caco-2 cells *in vitro*. We mimiked stomach transition by acid-treatment of two representative GRM followed by analysis of their physicochemical properties. No significant changes in the material properties or cell viability of exposed Caco-2 cells in respect to untreated GRM could be detected. Furthermore, we explored the interaction of four different GO and Caco-2 cells to identify relevant physicochemical properties for the establishment of a material property−biological response relationship. Despite close interaction with the cell surface and the formation of reactive oxygen species (ROS), no acute toxicity was found for any of the applied GO (concentration range 0−80 µg ml^{-1}) after 24 h and 48 h exposure. Graphene nanoplatelet aggregates led to low acute toxicity at high concentrations, indicating that aggregation, the number of layers or the C/O ratio have a more pronounced effect on the cell viability than the lateral size alone.

Introduction

Graphene as the most prominent member of the family of 2D materials has attracted enormous attention due to its unique combination of properties which offers a high technological potential for a broad variety of applications.[1,2] Graphene and several Graphene-related materials (GRM) are commercially available in various degrees of quality. Generally GRM can be produced by top-down approaches,[3–6] bottom up approaches,[7–9] reduction or functionalisation of other GRM[10,11] and transformation of other carbon nanomaterials.[12]

[a]*Laboratory for Particles-Biology Interactions, Swiss Federal Laboratories for Materials Science and Technology (Empa), Lerchenfeldstrasse 5, CH-9014 St. Gallen, Switzerland. E-mail: melanie.kucki@empa.ch, peter.wick@empa.ch*
[b]*Laboratory for Advanced Fibers, Swiss Federal Laboratories for Materials Science and Technology (Empa), Lerchenfeldstrasse 5, CH-9014 St. Gallen, Switzerland*
[c]*Université de Toulouse; CNRS, UPS, INP; Institut Carnot CIRIMAT, 118, Route de Narbonne, F-31062 Toulouse Cedex 9, France*
[d]*Istituto per la Sintesi Organica e la Fotoreattività, Consiglio Nazionale delle Richerche (CNR), Via P. Gobetti 101, 40129 Bologna, Italy*
[e]*Nano Cell Interactions, INM - Leibniz Institute for New Materials, Campus D 2.2, D-66123 Saarbruecken, Germany*
[f]*Departamento de Química Orgánica, Facultad de Ciencias y Tecnologías Químicas-IRICA, Universidad de Castilla-La Mancha, 13071 Ciudad Real, Spain*

Graphene oxide (GO), a subclass of GRM exhibiting oxygen-containing functional groups, has been identified as a promising candidate for biomedical applications such as tissue engineering, drug delivery, cancer treatment and biosensing.[13–15] The presence of oxygen functional groups facilitates the dispersibility in aqueous environment and enables the covalent functionalization with several different drugs, polymers and fluorescence labels by various chemical routes.[16,17] However, the public acceptance of every new technology is always coupled to its benefits and safety. The rapid development of graphene-based technology and expected large distribution has raised a lively safety discussion. There is great interest and attention on graphene not only in the academic community, but also in social media.[18] Despite a steadily increasing number of publications regarding the biological effects of GRM, especially GO, there is little consensus on the effect on human and environmental health.[19] Both the inconsistency of experimental results and a generic use of the term graphene for several different GRM have led to confusion.[20] A recently proposed classification framework aims to group different GRM by three main parameters (the average lateral dimension, the number of layers and the amount of oxygen as an indicator for oxidation) and to understand the relationship between GRM-structure and biological effects.[21] Similar to other nanomaterials the physicochemical properties and quality of GRM can highly influence the type and strength

of the biological response. Despite several *in vivo* studies, as summarized and analysed recently by Bussy *et al.*[22] a systematic investigation to correlate GRM properties and their biological effects with respect to the exposure route (inhalation, oral, dermal, intravenous) as well as their fate within the exposed organism is missing. From the occupational health perspective there are several exposure routes for workers towards GRM: inhalation, dermal contact and/or ingestion. Among these, inhalation is regarded as the most relevant way of unintended entrance of GRM into the human body. Therefore it is not surprising that a majority of published studies, except those addressing intravenous application for biomedical research, has addressed the possible impact of GRM on cells of the respiratory tract *in vitro*, as well as *in vivo*.[23,24] Nevertheless, information on the fate of these materials in the lungs and the possible induced biological effects is very limited. Next to the lungs, scant attention has been given to other biological barriers which are likely exposed to GRM. The gastro-intestinal (GI) tract can not only be exposed by direct ingestion of GRM, but also by indirect ingestion of formerly inhaled GRM. Trapped in the mucus of the respiratory system foreign bodies are transported upwards by ciliary movement, a process called the "mucociliary elevator", and can be finally either coughed out or swallowed down. In addition, potential application of GRM in food packaging and contamination of drinking- or surface water, are likely scenarios how GRM could gain access to the human GI-tract.

Nanomaterials that enter the alimentary tract are exposed to a series of different environments before they reach the intestine. Several factors such as pH, ionic strength, digestive enzymes, surface active compounds, physical forces, type and amount of food intake as well as microbes have the potential to induce changes to the physicochemical properties of the nanomaterial. Due to this complexity it is not clear which factors have the strongest influence on the nanoparticles. However, it is very likely that the acidic conditions within the stomach are among the most relevant factors. As every change in the physicochemical properties of the GRM has the potential to modulate the induced biological response, it is important to assess any possible change that can occur before the material reaches the cells or tissue of interest. Nevertheless, there is lack of information regarding GRM behaviour under physiologically relevant acidic conditions. Furthermore there has been no detailed investigation of the possible impact of GRM on the gastro-intestinal tract. Only very few studies with a small selection of GRM have addressed the interaction of GRM with intestinal cells *in vitro*.[25] However, the mucosal barrier of the intestinal tract is one of the most important biological barriers within the human and animal body. It serves multiple tasks, such as nutrient uptake, defence against pathogenic bacteria and maintenance of tolerance against commensal bacteria. Loss of intestinal homeostasis can result in uncontrolled entrance of pathogens and food antigens as well as in reduced nutrient supply, which in turn can lead to severe health complications and disturbance of the entire organism.

Therefore the aim of this study is to acquire a systematic understanding of the biological effects of GRM on cells of the human intestinal tract. For this purpose we selected and characterized graphene oxides (GO) of different sources and quality and explored their interaction with non-confluent Caco-2 cells. The Caco-2 cell line is derived from human colon adenocarcinoma and one of the gold-standards for *in vitro* studies regarding the intestinal tract with wide-spread application in pharmaceutical research. The selection of GO presented here offers a direct comparison of commercial and research grade materials, research-grade GO obtained by the same production method but with different lateral dimensions, as well as of commercial GO obtained from two different starting materials. To mimic stomach transition, exemplarily one selected GO, as well as graphene nanoplatelets aggregates (GNP) as benchmark GRM, were incubated under physiologically relevant acidic conditions *in vitro* followed by material characterization, especially focusing on determination of the surface functionalization (C/O ratio), introduction of defects and changes in material morphology. As there is no information available on the exposure dose of GO in the intestinal tract we selected a rather broad dose range up to a concentration of 80 μg GO per ml. It has to be noted that 80 μg GO per ml is already assumed to reflect an over-dose situation and that the expected exposure dose range is probably significantly lower. The obtained results will help to identify relevant physicochemical properties for the establishment of a material property–biological response relationship.

Results and discussion

Physicochemical properties of GO and GNP

To understand the correlation of the physicochemical properties of GO and the biological effects, we selected a set of four different GO samples produced by modified Hummers method. Two GO samples (GO1, GO4) were obtained from commercial sources in addition to two graphene oxides (GO2, GO3) produced in research laboratory. GO1, GO2 and GO3 were derived from graphite, whereas graphitic nanofibers (GANF©) were the starting material for GO4. As exfoliation is connected to the application of ultra-sonication which leads to random fragmentation of the GO sheets,[26] all GO samples exhibited poly-dispersed lateral sheet size. The commercial graphene oxide GO1 showed the largest lateral size distribution with a range of several tens of micro-meters. The commercial graphene nanoplatelets (GNP), applied as benchmark material for the digestion procedure, consisted of small and large flakes which were already fused to larger aggregates when received as powder from the manufacturer (see ESI†). Dispersion of hydrophobic GNP in water was improved by the application of sodium cholate, salt of a natural primary bile acid which is present in the human intestine and plays an important role in the digestive process, especially in the absorption of dietary fats. Bile acids are frequently used to disperse graphene in aqueous dispersions.[27,28] Short-time bath-

Table 1 Overview on the physicochemical properties of applied graphene-related materials (GRM)

Material type	Graphene oxide				Aggregated graphene nanoplatelets
GRM	GO1	GO2[29]	GO3[29]	GO4[c]	GNP
Source	Commercial	Research	Research	Commercial	Commercial
Preparation	Modified Hummers method	Modified Hummers method	Modified Hummers method	Modified Hummers method	Microemulsion
Starting material	Graphite	Natural graphite	Natural graphite	Graphite nanofiber (GANF©)	Natural graphite
Size distribution/ lateral dimension	1–40 μm (SEM) (300–800 nm, AFM[b])	360 ± 188 nm (AFM), some flakes larger than 1 μm	150 ± 44 nm (AFM)	20 nm–1.4 μm (TEM)	Aggregate size 1–10 μm; mean ~5 μm (SEM) (1–2 μm, AFM[b])
Number of layer/ thickness	Few to single layer (0.7–1.2 nm[b])	Monolayer/ 1.1 ± 0.1 nm	Monolayer/ 1.1 ± 0.1 nm	Few to single layer	Aggregate thickness up to 5 μm; 5–10 layers (shape of the Raman 2D band) (<4 layers; <4 nm[b])
Raman ID/IG ratio	1.19 ± 0.08 (633 nm) 0.96 ± 0.02 (532 nm)	1.34 ± 0.06 (633 nm) 1.06 ± 0.01 (532 nm)	1.30 ± 0.06 (633 nm) 0.97 ± 0.02 (532 nm)	0.81 ± 0.05 ($n = 5$)	0.37 ± 0.07 (633 nm) 0.17 ± 0.11 (532 nm)
C/O ratio	1.7 ± 0.1 (XPS)	1.9	1.9	2.61 (XPS)	24.0 ± 2.5 (XPS)
Zeta-potential (mV)[a]	−39.4 ± 1.3	−44.0 ± 0.2	−43.9 ± 1.4	−37.7 ± 0.4	−62.6 ± 1.9

[a] Measured in ultra-pure water with potassium chloride (KCl) as background electrolyte. [b] According to information given by the manufacturer; further details are given in the ESI. [c] Further characterization data for GO4 can be found in Kurapati *et al.*[30]

sonication was applied to further improve dispersion. Nevertheless, short-time bath-sonication (<10 min) did not lead to dissociation of the graphene layers. Further sonication (long duration or high energy) was not applied in order to prevent significant changes in the material properties.

All graphene oxides did not require additional treatment and were either already obtained as aqueous dispersions or dispersed in endotoxin-free ultra-pure water. An overview of the physicochemical properties of the applied GRM is given in Table 1.

Physicochemical properties after *in vitro* digestion (acid-treatment)

Based on the fact that all nanomaterials entering the GI-tract have to pass through the stomach prior to any contact with intestinal cells, we explored the impact of physiological relevant acidic conditions as present in the stomach on the physicochemical properties of graphene-related materials *in vitro*. For this purpose, we selected two different commercially available GRM which highly differed in their physicochemical properties. GO1 was selected as representative for graphene oxides, whereas graphene nanoplatelet (GNP) aggregates were used to cover GRM with significantly different properties, especially carbon-to-oxygen ratio (C/O) and layer number. Selected GRM were incubated in 0.1 M hydrochloric acid (HCl) for 2 hours at 37 °C under mild agitation. As a control, aliquots of the same GRM were incubated in water instead of hydrochloric acid at similar conditions to exclude any changes in the material properties independent of the acidic conditions. After treatment, GRM were harvested by centrifugation, re-dispersed and neutralized in phosphate buffered saline (PBS, pH 6.8), washed and transferred to ultra-

pure-water prior to material characterization. Physicochemical characterization of the acid-treated GRM and the respective control (water-treated) GRM was performed by SEM analysis, zeta-potential measurement, X-ray photoelectron spectroscopy (XPS) analysis and Raman spectroscopy. Results are summarized in Table 2. SEM analysis did not indicate major changes in the GRM morphology, neither for GO1, nor for GNP as shown in Fig. 1. Control samples and acid-treated samples showed no obvious differences. The zeta-(ζ)-potential of GO1 (as received & acid-treated) in ultra-pure water with potassium chloride (KCl) as background electrolyte showed identical values of −39 mV, giving no hints towards altered surface charge. The zeta-(ζ)-potential of GNP was between −50 and −62 mV, and therefore more negative than that of GO1. The presence of sodium cholate, which was used as surfactant

Table 2 Physicochemical properties of GRM after acid-treatment

Sample		C/O[a]	Zeta-(ζ)-potential[b] (mV)	Raman ID/IG bands (633 nm)
GO1	As received	1.7 ± 0.1	−39.4 ± 1.3	N.D.
	Control	1.9 ± 0.1	N.D.	1.19 ± 0.08
	Acid treated	1.8 ± 0.1	−39.7 ± 3.7	1.22 ± 0.12
GNP[c]	As received	24.0 ± 2.5	−62.6 ± 1.9	N.D.
	Control	25.0 ± 2.5	−54.6 ± 4.1	0.37 ± 0.07
	Acid treated	24.4 ± 2.5	−56.7 ± 1.8	0.31 ± 0.11

[a] Determined from the XPS survey spectra. The estimated error is ±0.1 and ±2.5 for GO1 and GNP samples, respectively, and results from the uncertainty of the determination of the elemental concentrations from the XPS in the order of 10% under our experimental conditions. [b] Measured in ultra-pure water with potassium chloride (KCl) as background electrolyte. [c] Contains primary bile salt sodium cholate (SC); N.D. = not determined.
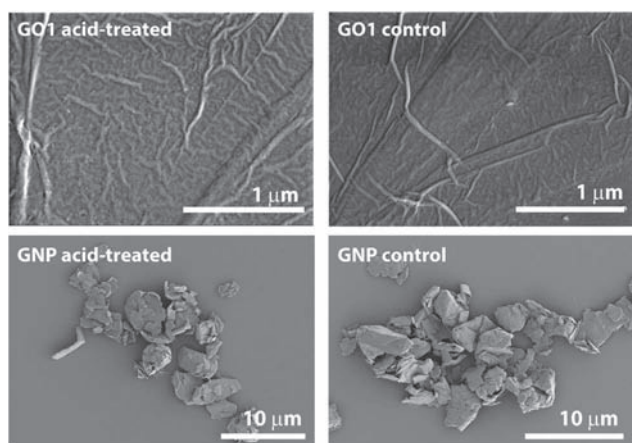
Fig. 1 Representative SEM images of the GRM morphology with or without acid-treatment.

to achieve dispersion of GNP in aqueous solution, had no to minor influence on the zeta-(ζ)-potential of the GNP (see Table S4b in ESI†) and is therefore not responsible for the highly negative values. After acid-treatment of GNP, the absolute zeta-(ζ)-potential was reduced to a slightly smaller value.

The elemental composition of the GRM, in particular the carbon to oxygen ratio (C/O) was characterized by XPS. For each of the two materials, GO1 and GNP, the surface of the material was characterized in the as received form, the control sample, as well as after acid-treatment. In addition, high resolution spectra for the elements carbon and oxygen were recorded in order to detect possible chemical changes. For the GO1 sample as received, the survey scan revealed the elements carbon and oxygen in significant concentrations, whereas small amounts ($\leq$1 atomic%) of nitrogen, silicon and sulfur were also detected, probably resulting from the GO production and/or storage. For the GNP sample as received, only the elements carbon and oxygen were present. Table 2 summarizes the C/O ratios calculated from the oxygen and carbon concentrations determined from the XPS survey spectra. The C/O ratio for the GO1 sample as received resulted to 1.7, in agreement with literature values for commercial graphene oxide.[31–33] A small increase of the C/O ratio was found after GO1 was acid-treated as well as for the control sample. For further information see Fig. S5 in the ESI.† As expected, the C/O ratio was significantly higher (above 20) for the GNP samples. Only small concentrations of oxygen were present in the GNP. No significant differences were found between the GNP sample as received, the acid-treated GNP and the control GNP sample. The values are all well within the estimated uncertainty of ±2.5. Further information to the XPS measurements is given in the ESI.†

Raman spectroscopy of GO1 and acid-treated GO1 did not give evidence for significant differences after treatment of GO1 under physiological relevant acidic conditions (*cf.* Fig. S6-c and S6-d in ESI†). However in the case of GNP, a decrease in the

D/G intensity ratio, on average 25%, was evidenced after acid-treatment (*cf.* Fig. S6 in ESI†). Such a decrease of the ratio for a constant G peak width usually corresponds to a lower level of defects in the samples.[34] This could result of a selective degradation of the sites containing the highest density of defects, sites which should also have the highest chemical reactivity. But, according to the statistical tests performed on the measurements (*cf.* Experimental section), the possibility that this observation comes from the heterogeneity of the starting GNP material (evidenced by measuring the Raman signal at different places) cannot be excluded.

The probability that the GRM was not modified by the treatment is in fact about 8%, which is not negligible. Indeed, as presented in Table 2, the standard deviation on the measured D/G intensity ratio is very high, about 30%.

In summary, we can conclude that the acid-treatment of the two selected GRM, GO1 and GNP, did not result in major changes in the material properties. At least for the GO this is not surprising, as production of GO by classical methods such as Brodie, Staudenmaier and Hummers method involves sulfuric acid (H_2SO_4) and nitric acid (HNO_3).[3] Nevertheless, our results demonstrate that pristine GO and GNP are relatively inert materials which appear to be not highly affected by the acidic conditions (pH $\leq$ 2, fasted state, 2 h, 37 °C) during stomach transition.

Interaction of acid-treated GRM with the Caco-2 cell surface

In a next step we assessed the interaction of acid-treated and control GRM derived from the *in vitro* digestion procedure with the Caco-2 cell surface. As the physicochemical characterization of acid-treated and control GRM did not reveal major changes in material properties, we did not expect significant differences in the interaction with the cell surface after exposure to GRM. As shown in Fig. 2 the interaction of the acid-treated GRM and the cell surface showed no distinctive features in comparison to the respective control GRM. For GO1, in both samples (acid-treated and control) GO sheets were primarily found folded and wrinkled, reminiscent of crumbled paper. There were no visible hints towards a possible damage of the cell surface by the GO sheets. Cell morphology of Caco-2 cells after exposure to GO1 samples (acid-treated and control samples) did not show significant alterations in comparison of untreated Caco-2 cells. Similar observations were made for all GNP samples. GNP aggregates of different shapes but in the usual size range of 1–10 μm were found associated with the Caco-2 cell surface. For both GO1 and GNP a few observations were made which might be hints towards attempts of cellular uptake as shown in Fig. S7 and S8 in ESI.† If these events are real uptake events or rather overgrowth of the GRM has to be clarified by detailed analysis in future investigations.
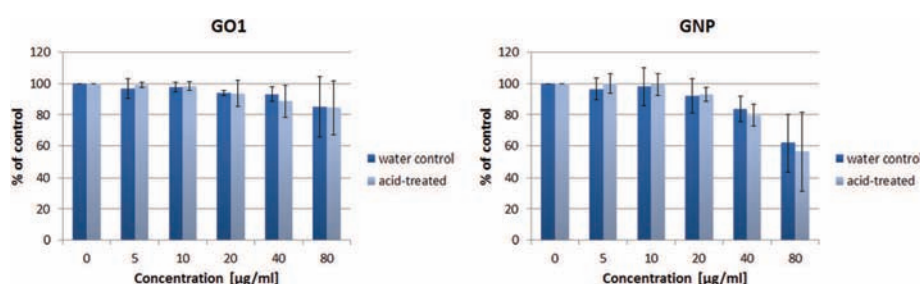
Cell viability of Caco-2 cells after exposure to acid-treated GRM

The possible impact of GRM exposure on Caco-2 cells was assessed by measurement of the metabolic activity *via* MTS (3-(4,5-dimethylthiazol-2-yl)-5-(3-carboxymethoxy-phenyl)-2-(4-
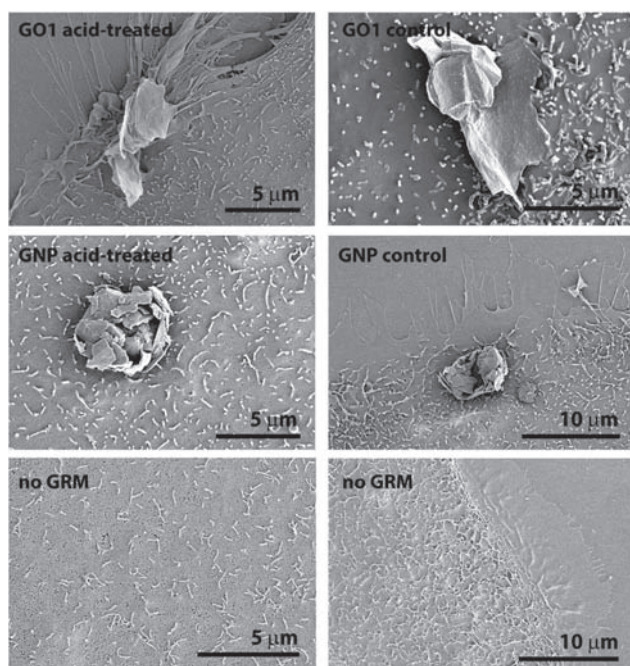
Fig. 2 Representative SEM images of Caco-2 cells after exposure to 20 μg ml^{-1} acid-treated GRM or the respective control-GRM for 24 h, as well as of untreated control cells.

sulfophenyl)-2*H*-tetrazolium, inner salt) assay. Cytotoxic potential of a sample was reached when the metabolic activity decreased to less than 70% of the control cells. For GO1, exposure to the acid-treated sample or the respective control sample for 24 h resulted in a concentration dependent slight decrease in mean viability of Caco-2 cells as shown in Fig. 3. Nevertheless, even at highest GO concentration applied (80 μg GO per ml) the cell viability remained above 80% in relation to the unexposed control cells. For GNP, the decrease in cell viability was more pronounced. Mean cell viability decreased to around 60% for the highest concentration applied, indicating low acute toxicity. Comparison of the viability of Caco-2 cells exposed to acid-treated GRM and the respective water-treated control sample did not reveal any differences in metabolic activity. Light microscopy images also showed the absence of visible differences in cell morphology between control cells

and cells exposed to water-treated or acid-treated GRM (see Fig. S9 and S10 in ESI†). Therefore, as confirmed by material characterization, incubation of GRM under acidic conditions reflecting the pH value in the stomach did not result in significant changes of the material properties or the cellular activity of exposed intestinal cells *in vitro*. Nevertheless, prior to this study it has not been demonstrated yet that the acidic conditions in the stomach do not affect graphene oxide properties. The results indicate that acid pre-treatment of pristine GO (without further functionalization) to mimic stomach transition is not mandatory, at least when the production method already involved treatment with acids.

Cell surface interaction of different GO samples

Detailed characterization and knowledge of the material properties of GRM enables a comprehensive correlation of the physicochemical properties and possible biological effects. To acquire a systematic understanding of the interaction of a certain GRM type with human intestinal cells, non-confluent Caco-2 cells were exposed to the above mentioned selection of different graphene oxides (GO1–4). In addition, untreated GNP was implemented for comparison. Based on the results obtained previously, the following investigations were performed without acid-treatment, as the involved GO samples were produced by modified Hummers method. Non-confluent Caco-2 cells were exposed directly to the untreated GO samples.

SEM analysis of Caco-2 cells after exposure to different GO samples showed a close interaction of the GO sheets and the cell membrane. Well exfoliated GO sheets showed the tendency to align in parallel to the cell surface, especially in areas where the cell surface was relatively smooth with a low amount of cell protrusions. In several cases GO sheets could only hardly be distinguished from the cellular membrane as shown in Fig. 4 for GO2. Similar observations were made by Russier *et al.* for GO with human and murine macrophages and described as so-called "mask-effect".[35] In addition to the parallel alignment of the GO sheets, several sheets comprising numerous folds and wrinkles were found on the cell surface, especially near the edges of Caco-2 islets. In this region Caco-2 cells showed numerous wave-like cell protrusions. All GO samples showed well exfoliated sheets. Nevertheless, GO4 fre-
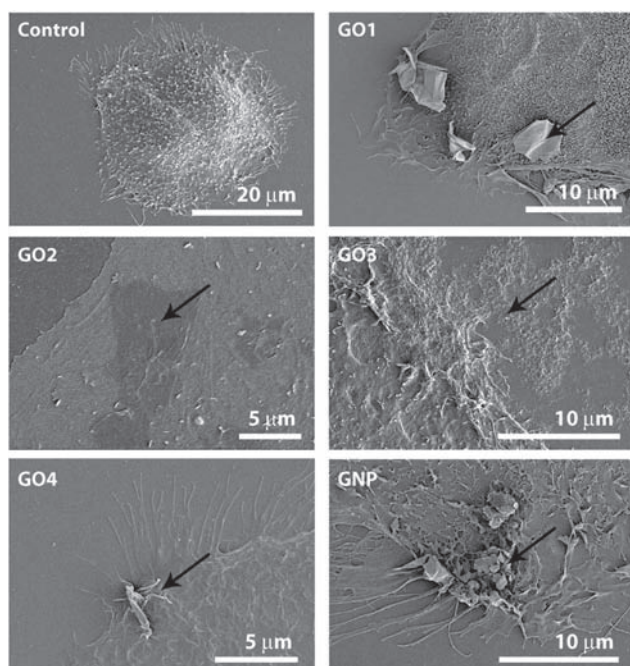

Fig. 3 Cell viability of Caco-2 cells after exposure to acid-treated and control GRM samples for 24 h; left: GO1, right: GNP; all materials were tested in three independent experiments with three replicates for each concentration. Results are shown as mean and standard deviation.

Fig. 4 Representative SEM images of Caco-2 cells after exposure to different GRM for 24 h with an applied concentration range of 10–40 μg mL⁻¹ GRM; images shown for 10 μg ml⁻¹ GO1 and GO4; 20 μg ml⁻¹ GO2 and GNP, as well as 40 μg ml⁻¹ GO3 respectively. GO3 sheet assemblies are visible next to the cells on the glass substrate in the upper right corner. Black arrows point towards the respective GRM.

quently exhibited some puff paste structured sheet assemblies. As described before, larger GNP aggregates were frequently found attached to the cell surface, again predominantly near the edges of Caco-2 islets. Exposure of Caco-2 cells to the four different GO, as well as the GNP, in a concentration range from 10–40 μg ml⁻¹ GRM for 24 h did not result in any visible morphological alterations of the cells or hints towards altered cell turnover. Furthermore cells frequently showed affinity to GO deposited on the glass substrate. As mentioned before, for GO1 and GNP few single events were observed which might indicate cellular uptake (Fig. S7 and S8 in ESI†).

Induction of reactive oxygen species by GO and GNP

Studies with other carbon-based materials have shown that these materials can induce the formation of reactive oxygen species (ROS).[36,37] ROS such as hydrogen peroxide (H_2O_2) are highly reactive molecules which are involved in intra- and intercellular signalling. Up to a certain limit ROS-formation can be outbalanced by the cellular antioxidant defence. Nevertheless, imbalance due to elevated ROS levels can lead to severe damage of lipids, proteins and nucleic acids, which can in turn result in inflammatory reactions, genotoxicity or cell death. Therefore we assessed the possible GRM-induced formation of ROS by 2′,7′-dichlorodihydrofluorescein diacetate (H_2DCF-DA) assay, a common assay previously applied with multi-walled carbon nanotubes (MWCNTs)[36] and graphene shells.[37] Fig. 5 shows the results obtained for Caco-2 cells

exposed to different GO and GNP for 2 hours. 3-Morpholinosydnonimine hydrochloride (SIN-1) served as qualitative positive control applied at a concentration of 150 μM in HBSS. In addition, sodium cholate in water was applied as vehicle control for GNP dispersions. The results clearly show that all applied GO, as well as the GNP, induced the formation of ROS in Caco-2 cells. Nevertheless, despite slight differences in the intensity of ROS formation found for individual GRM quantitative comparison is not possible due to concentration-dependent quenching of the DCF fluorescence in the presence of GO1, GO2, GO4 and GNP (see Fig. S14 and S15 in ESI†).

Similar decrease in fluorescence intensity was already reported for high concentrations of MWCNTs[36] and graphene shells.[37] In contrast, GO2 exhibited fluorescence enhancement activity at low and medium concentrations, as well as fluorescence quenching at high concentrations (see Fig. S15 ESI†). Interference by intrinsic fluorescence of the GO and GNP could be excluded (see Fig. S12 and S13 ESI†). Further control experiments showed that all GRM were able to transform the de-acetylated H_2DCF molecule into a fluorescent product, indicating the production of ROS by the GRM in the absence of cells (see Fig. S16 ESI†). These results are again in line with findings previously reported for MWCNTs[36] and graphene shells.[37] Therefore, at least part of the ROS detected in the cell-based assay results from the activity of the GO or GNP alone.

Cell viability of Caco-2 cells after exposure to a whole selection of GO representing research grade and commercial GO

We further investigated whether the induced ROS formation can reach sufficient levels to have an impact on the cell viability of proliferating Caco-2 cells. Exposure to four different graphene oxides (GO1–4) for 24 h and 48 h resulted in a slight dose dependent decrease of the metabolic activity of Caco-2 cells, as determined by the application of the MTS-assay. Even at the highest GO concentration (80 μg ml⁻¹) applied the mean cell viability was above 80% for 24 h as well as 48 h exposure time for all GO samples, again indicating no acute toxicity of the GO for Caco-2 cells. To assess possible loss of cells after exposure to GO due to an increase in cell death, the total number of adherent Caco-2 cells was measured by modified lactate dehydrogenase (LDH) assay. After exposure to GO cells were washed with phosphate buffered saline and lysed for 60 minutes by addition of 9% triton-X 100 in PBS. The cell number was determined by measurement of the total LDH release after complete cell lysis. Release of LDH was linear to the number of lysed cells. As shown in Fig. 6 no significant decrease in cell number indicating loss of cells after exposure to GO was found for any GO sample and concentration applied.

In summary the results indicate that acid pre-treatment of pristine GRM seems to be not mandatory. Nevertheless it is definitely advisory to perform equivalent acid pre-treatment in case the selected GO is further functionalized or loaded with drugs for drug delivery or cancer treatment. Detailed analysis of the stability of functionalization under gastric conditions is inevitable. It should be noted that the digestion procedure applied here can be seen as a starting point for further sys-
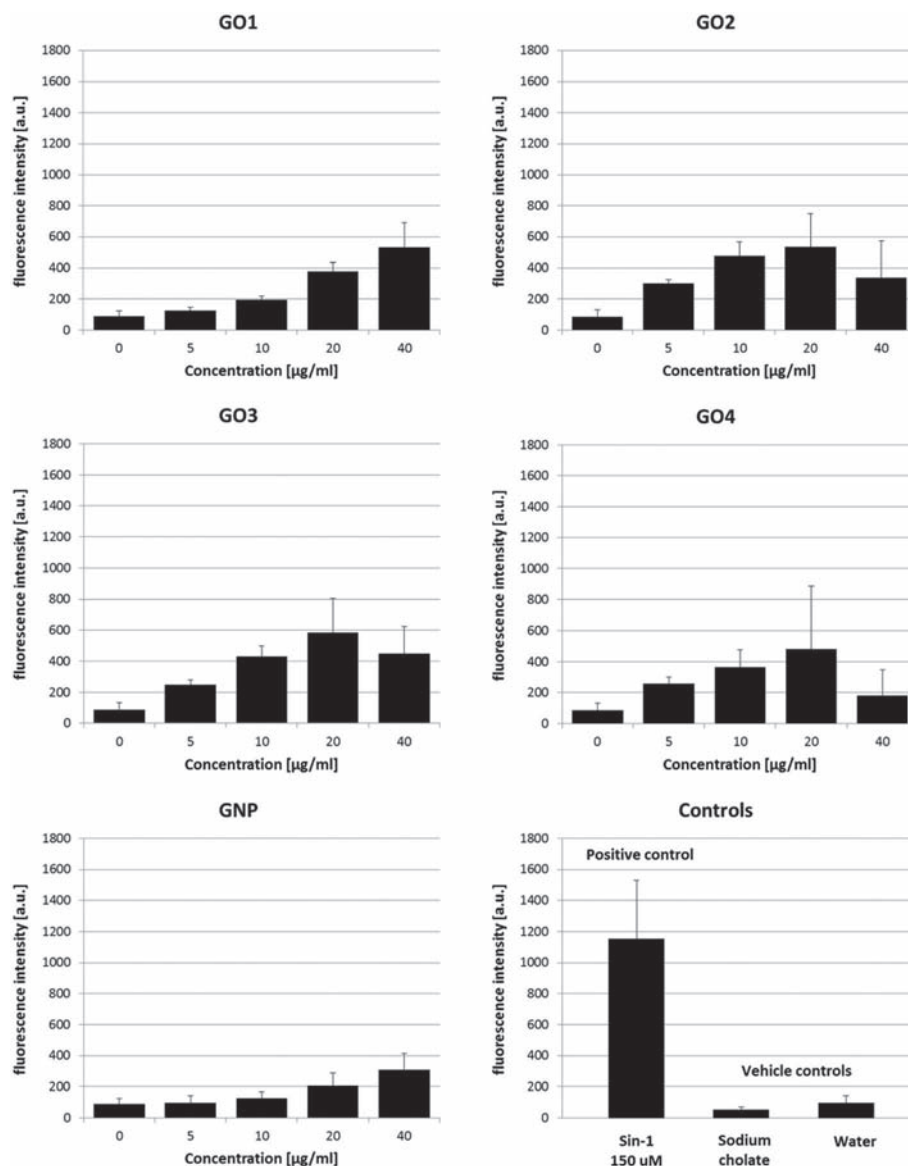
Fig. 5 H$_2$DCF assay: ROS formation after exposure of Caco-2 cells to 5–40 µg ml^{-1} of the respective GO or GNP. Sin-1 served as positive control. Aqueous solution with 0.1 mg ml^{-1} sodium cholate served as vehicle control for the GNP samples.

tematic investigation of relevant factors influencing the material properties. We considered the acidic conditions as an isolated factor. But *in vivo* gastric fluids consist of a large diversity of further factors, such as salts, proteins and enzymes, which alone or in combination can have an influence on the GRM properties. From the multitude of available simulated body fluids of the alimentary tract (*e.g.* saliva, gastric and intestinal fluids) appropriate protocols have to be selected resembling the *in vivo* situation under consideration (*e.g.* fasted state *vs.* fed-state).

Despite close interaction with the cell membrane and induction of ROS-formation, no GO, either with or without acid pre-treatment, led to acute toxicity towards non-confluent Caco-2 cells. These results are in line with those obtained for Caco-2 cells exposed to two graphene oxides of different lateral

dimension[25] or single walled carbon nanotubes (SWCNTs),[38] which can be regarded as rolled up graphene sheets. Two graphene oxides with different lateral size distributions also showed no acute toxicity to the lung epithelial cell line A549 when applied in concentrations up to 100 µg ml^{-1} GO.[39] The physicochemical characterization showed that GO obtained from different sources but produced by the same top-down method (modified Hummers method) did not show large differences in the C/O ratio and layer number, but in the lateral size distribution. Expected differences in cell response of Caco-2 cells in dependence of the lateral size distribution of the GO, could not be observed. In addition, the starting material (graphite or GANF®) also had no influence on the acute toxicity towards Caco-2 cells. This is in a way surprising since other studies with different cell types reported size
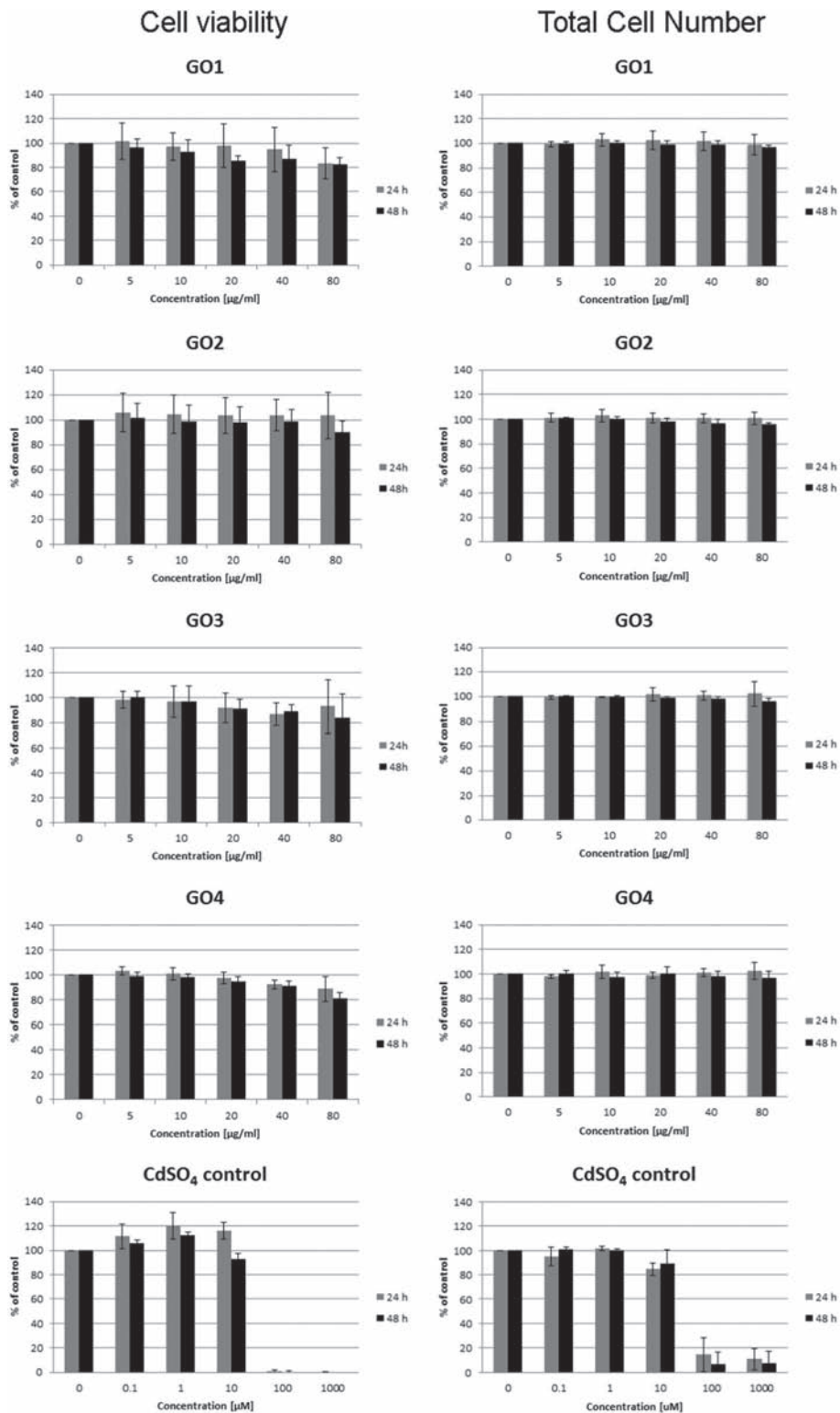
Fig. 6 Cell viability and total cell number of adherent Caco-2 cells after exposure to different GO samples for 24 h and 48 h. Cadmium sulphate (CdSO$_4$) served as chemical control for the assay performance. Cell viability and total cell number are both presented as percentage of control cells not exposed to GO. Results are shown as mean and standard deviation of 3–6 independent experiments.

dependent effects of GO.[39] But it should be noted that the size distribution of the applied GO is extremely large compared to other nanomaterials such as monodisperse silica nano-

particles. It cannot be excluded that certain sub-populations within the huge size range have a stronger effect than others. Pre-requisite for further analysis of the influence of the lateral

dimension would be the availability of GO with a very narrow size distribution, which is still a challenge to achieve. Large differences in the physicochemical properties, such as layer number and/or the C/O ratio, as it is the case between GO and GNP, led to visible changes in the level of acute toxicity towards Caco-2 cells but only at concentrations higher than 40 μg ml^{-1}. The influence of the layer number/thickness and the C/O ratio has to be further determined in future experiments.

Despite the lack of acute toxicity of GO and low acute toxicity of GNP at high concentrations, our results do not rule out that specific biological effects can be observed at sub-toxic GO levels. Further experiments regarding possible cellular uptake, loss of cellular functions and DNA damage have to be performed in future. Next to enterocytes the intestinal epithelium comprises several other types of cells (*e.g.* mucus-secreting goblet cells, antigen-sampling M-cells, entero-endocrine cells, Paneth cells, intestinal stem cells as well as intra-epithelial lymphocytes) with high variation in function and morphology which might show different interactions with GO. Even if these cell types occur in significant lower number compared to enterocytes which represent the majority of the cells of the intestinal barrier, further studies with these cell types (undifferentiated and differentiated, *in vitro* and *in vivo*) are needed to exclude any possible adverse effect of GO on the intestinal barrier. In addition, possible effects of chronic exposure of the intestinal barrier to GRM should be addressed.

Conclusions

The results of this study show that graphene oxides as well as graphene nanoplatelet aggregates are relatively inert towards physiological relevant acidic conditions and are likely to undergo stomach passage without significant changes in their physicochemical properties. Therefore acid pre-treatment of pristine GO is not required to investigate potential acute toxicity towards cells of the intestinal tract *in vitro*. Nevertheless, this should not necessarily be valid for GO functionalized with biomolecules or drugs for biomedical application. In this case careful assessment of the stability of the functionalization under relevant acidic conditions is recommended. The lack of acute toxicity of four different GO samples to non-confluent Caco-2 cells is very promising in respect to a possible biomedical application as well as important regarding unintended exposure. In contrast exposure of Caco-2 cells to high concentrations of GNP showed low acute toxicity, which indicate that physicochemical parameters such as layer number and C/O ratio seem to be critical for the level of biological response of Caco-2 cells towards GRM.

Experimental section

Materials, sources & production

Graphene oxide 1 (GO1; SLGO) and Graphene nanoplatelets (GNP; HDPlas™ GNPs Grade 4) were obtained from Cheap Tubes (Battleboro, 112 Mercury Drive, VT05301, USA; http://www.cheaptubes.com). Research grade graphene oxide samples GO2 and GO3 were prepared from graphite flakes by a modified Hummers method as described by Treossi *et al.*[40] The lateral size of the GO flakes can be tuned by changing the sonication time of the starting solutions, in particular in this work we used two graphene oxide solution sonicated 2 h (GO2) or 20 h (GO3) respectively. GO4 was obtained from Grupo Antolin-Irausa S.A. (Ctra. Madrid-Irún, Km. 244,8 – E09007 – Burgos, Spain).

Digestion of GRM

GO1 and GNP were incubated in 0.1 M hydrochloric acid (HCl) for 2 h in 37 °C under slight agitation. In parallel, GO1 and GNP were incubated in ultra-pure water under similar conditions as controls for the digestion procedure. After incubation, all samples were precipitated by centrifugation (10 min at 5000 rpm). The clear supernatant was exchanged by phosphate buffered saline (PBS) with pH 6.8 which resembles the pH values in the small intestine and served for neutralization. GRM were re-dispersed and washed twice with ultra-pure water by centrifugation prior to further use.

Scanning electron microscopy (SEM) analysis of GRM

For SEM analysis of the GRM morphology GRM were applied as received from the manufacturer. GRM powders or dispersions in ultra-pure water were applied on clean glass cover glasses (10 mm Ø, # 1, Menzel GmbH, Braunschweig, Germany) fixed on the SEM sample holder by conductive carbon strips to prevent direct contact of the carbon film and the carbon nanomaterial. Dispersions were dried at room temperature. All samples were sputter coated with 5 nm gold–palladium (Au/Pd = 80/20). Analysis was performed with SEM (Hitachi S-4800).

Zeta-(ζ)-potential measurements

The zeta-(ζ)-potential was measured with a Zeta Sizer Nano ZSP (Malvern Instruments, Worcestershire, UK) using disposable capillary cells (DTS1070, Malvern Instruments, Worcestershire, UK). For measurements, GRM dispersions were diluted to a concentration of 100 μg ml^{-1} in ultra-pure water, containing potassium chloride (KCl) as background electrolyte (end-concentration: 1 mM), 0.1 mg ml^{-1} sodium cholate containing 1 mM KCl (for GNP only) or cell-culture medium (MEM + 10% FBS). Particle dispersions were diluted 1 : 10 in medium. The zeta potential of GO1 was also measured after incubation in cell-culture medium and separation of the medium, according to the following steps: 30 min incubation in cell-culture medium, centrifugation (centrifuge 5418 Eppendorf, Hamburg, DE) of the samples at 16 000*g* for 1 h, aspiration of the supernatant and re-dispersion (1 min vortex) in ultra-pure water. Each sample was measured three times.

X-ray photoelectron spectroscopy (XPS)

XPS measurements were carried out with a Scanning XPS Microprobe (PHI VersaProbe II spectrometer, Physical Elec-

tronics) using monochromatic Al Kα radiation (1486.6 eV). The operating pressure of the XPS analysis chamber was below 5×10^{-7} Pa under the measurement conditions presented here. The spectra were collected at photoemission take off angles of 45° (with respect to the surface). Survey scan spectra (0–1100 eV) were acquired with an energy step width of 0.8 eV, acquisition time of 160 ms per data point and analyser pass energies of 187.85 eV. Higher resolution narrow spectra for the elements carbon C1s (278 eV to 298 eV energy range) and oxygen O1s (523 eV to 543 eV energy range) were acquired with energy step widths of 0.125 eV, acquisition times of 3.2 s (carbon) and 2.56 s (oxygen) and analyser pass energies of 29.35 eV. Under these experimental conditions (pass energies), the energy resolution (FWHM, full width at half maximum height) measured on silver Ag 3d5/2 photoemission line is 2.4 eV and 0.7 eV, respectively. The total acquisition times were approximately 4 min for survey scans and 16 min for the two high-energy resolution elemental scans together, which achieve an adequate signal-to-noise ratio without observable X-ray radiation damage to the samples. Each sample was analysed at a randomly chosen spot using a micro-focused, scanned X-ray beam with a diameter of 200 μm (operated at a power of 50 W at 15 kV). The 180° spherical capacitor energy analyser was operated in the fixed analyser transmission mode (FAT). The GRM samples (acid treated and control) have been attached to clean and sterile cover glasses, whereas the as received GRM were pressed onto an indium foil. The cover glasses as well as indium foil were then placed on a 2.5 cm diameter sample holder. In order to compensate possible sample charging, dual beam charge neutralization with a flux of low energetic electrons (1.4 eV) combined with very low energy positive Ar-ions (10 eV) was used. The binding energy is referenced to the C–C, C–H hydrocarbon signal C 1s at 285.0 eV. Curve fitting (least-squares fit routines) was carried out with CasaXPS software version 2.3.16. Thereby, a mixed Gaussian–Lorentzian product function (constant ratio of 70% Gaussian and 30% Lorentzian) was used to de-convolute the XP spectra. During the fitting process, the positions on the binding energy scale were constraint to corresponding literature values.[33] Atomic concentrations were calculated from XPS peak areas after subtracting a Shirley type background. Thereby, tabulated PHI sensitivity factors[41] corrected for our system's transmission function and spectrometer geometry (asymmetry function) have been used for quantification.

Raman spectroscopy

Raman spectroscopy was performed on a confocal Raman microscope Labram HR800 Horiba Yvon Jobin, at 2 different laser wavelengths (red: 633 nm; green: 532 nm; hole: 100 μm, 100× magnification, 5 accumulations of 5 s each, between 1000 and 3000 cm^{-1}). The use of two different wavelengths is important because the shape and intensity ratios depend on the laser energy. Samples were prepared by drop casting on microscope glass slides. For each kind of treated GRM, 3 slides were studied, with about 7 measurements on agglomerates of different sizes. Significance of observed differences was then estimated with Student's t-tests supposing a normal distribution of measurements around the value really characterising each sample. Such a test is preconized to compare the means from two small and independent samples. Previously, the equality of the variances of each assay of measurements had been verified with F-test.

Cell culture

Caco-2 cells derived from human colorectal adenocarcinoma were obtained from ATCC (Product ATCC®HTB-37™, ATCC, Manassas, VA, USA). Caco-2 cells from cryogenically-preserved stocks were sub-cultured at least twice before the experiments. Cells were grown in Minimum essential medium (MEM, Ref. M2279, Sigma-Aldrich Chemie GmBH, Steinheim, Germany) supplemented with 10% non-heat inactivated fetal calf serum (FCS), 1% non-essential amino acids (NEAA), 1% L-glutamine, 1% penicillin–streptomycin–neomycin (PSN) and incubated in a humidified atmosphere with 5% CO$_2$ at 37 °C. Routinely cells were sub-cultured twice a week at 70–80% confluence by 0.5% trypsin-EDTA. To avoid pheno- and genotypic changes during cultivation of the cells, cells used for experiments were limited to 30 passages after thawing.

Scanning electron microscopy (SEM) analysis of Caco-2 cells

Caco-2 cells were seeded on clean and sterile cover glasses (15 mm Ø, # 1, Menzel GmbH, Braunschweig, Germany) in 12-well cell culture plates at a cell density of 1×10^5 cell per well, allowing attachment of the cells for 24 h prior to the experiments. Cells were exposed to 10–40 μg ml^{-1} GRM in supplemented cell culture medium for 24 h in parallel to control cells without GRM exposure. After exposure cells were washed twice with pre-warmed phosphate buffered saline (PBS). Cells were prepared by chemical fixation adding modified Karnovsky fixation solution (4 g paraformaldehyde (CAS 30525-89-4), 50 ml aqua bidest, 5 ml glutaraldehyde 50% (CAS 111-30-8, toxic if swallowed or if inhaled, causes severe skin burns and eye damage!), 45 ml phosphate buffered saline without glucose and pH 7.4) and incubation at room temperature for 1 hour. Samples were washed twice with PBS. Dehydration of the samples was performed by ascending ethanol series (50–100% ethanol) followed by hexamethyldisilizane (HMDS, CAS 999-97-3, harmful if swallowed or if inhaled, toxic in contact with skin!) treatment. Samples were dried overnight in a fume hood and stored in a desiccator until sputter coating with 10 nm gold–palladium (Au/Pd = 80/20).

Detection of reactive oxygen species (DCF assay)

The formation of reactive oxygen species (ROS) was determined by 2′,7′-dichlorodihydrofluorescein diacetate (H$_2$DCF-DA, CAS 4091-99-0) assay as described in ref. 37 with small changes. In brief, Caco-2 cells were seeded with 1×10^4 cells in 100 μl of complete cell culture medium per well in a 96 well plate and grown overnight under standard cell culture conditions. On the following day, cells were loaded with 50 μM H$_2$DCF-DA in Hank's buffered salt solution (HBSS) in a humidified atmosphere at 37 °C for 60 minutes. Cells were

washed twice with pre-warmed HBSS. In each case Caco-2 cells were exposed to 100 μl of the GRM dispersions with concentration ranges from 0–40 μg ml^{-1}. 3-Morpholinosydnonimine hydrochloride (SIN-1, CAS 16142-27-1) served as positive control applied at a concentration of 150 μM in HBSS. After 2 hours incubation time fluorescence intensities were measured at 485 nm excitation and 528 nm emission wavelengths by FLx800 fluorescence microplate reader (BioTek Instruments). Control experiments in the absence of cells were performed to determine possible ROS generation by the GRM, intrinsic GRM absorbance and fluorescence, as well as fluorescence quenching (see ESI†).

Cell viability

Cell viability of Caco-2 cells after exposure to different GO was assessed by measurement of the metabolic activity *via* MTS (3-(4,5-dimethylthiazol-2-yl)-5-(3-cyrboxymethoxy-phenyl)-2-(4-sulfophenyl)-2*H*-tetrazolium, inner salt) assay obtained as Cell-Titer96 Aqueous One Solution from Promega Corporation (2800 Woods Hollow Road, Madison, WI 53711-5399, USA). The assay was performed according to the manufacturer's protocol with slight changes to consider intrinsic GRM absorbance. Cells were seeded in 96-well plates (tissue culture test plate 96F, Ref. 92096, TPP® Techno Plastic Product AG, Switzerland) at a cell density of 1×10^4 cells in 100 μl of complete cell culture medium per well. Cells were grown overnight at standard cell culture conditions. The day after, cells were exposed to respective GRM diluted in complete cell culture medium at a concentration range of 0–80 μg ml^{-1} GRM for 24 and 48 hours. Cadmium sulphate (CdSO$_4$) was applied as positive control in a concentration range of 0–1000 μM. After exposure the medium was replaced by 120 μl MTS working solution (20 μl MTS reagent plus 100 μl phenol-red free RPMI-1640). Directly after addition of the working solution absorbance was measured at 490 nm to obtain background absorbance values (*t*0 value) considering intrinsic absorbance of residual GRM. Cells were incubated under standard cell culture conditions for 60 min. Final absorbance (*t*1 value) was measured at 490 nm wavelengths. Absorbance values (*t*1 values) were corrected for intrinsic GRM absorbance by subtraction of the *t*0 values. Data is presented as mean and standard deviation of at least three independent experiments.

Analysis of total number of adherent cells (modified lactate dehydrogenase [LDH] assay)

Total number of adherent cells was assessed by the CytoTox96® Non-Radioactive Cytotoxicity Assay (Ref. G1780, Promega Corporation, 2800 Woods Hollow Road, Madison, WI 53711-5399, USA) according to the manufacturer with slight modification to consider intrinsic GRM absorbance. For this purpose cells were seeded in 96-well plates at a cell density of 1×10^4 cells in 100 μl of complete cell culture medium per well and grown overnight at standard cell culture conditions. Cells were exposed to 0–80 μg ml^{-1} GRM diluted in complete cell culture medium for 24 and 48 hours. Cadmium sulphate (CdSO$_4$, CAS 10124-36-4, toxic if swallowed, fatal if inhaled)

served as positive control in a concentration range of 0–1000 μM. After exposure cells were washed twice with pre-warmed phosphate buffered saline. All cells were lysed by the addition of lysis solution (9% Triton-X 100, CAS 9002-93-1) and incubation at 37 °C for 45 min. After complete cell lysis absorbance was measured at 490 nm wavelength to obtain background absorbance values (*t*0 value) considering intrinsic absorbance of residual GRM. Assay reagent was added to each well. The 96-well plates were incubated at room temperature for 30 minutes. After 30 min incubation time stop solution was added to stop reaction. Final absorbance (*t*1 value) was measured at 490 nm wavelength. Results were corrected for intrinsic GRM absorbance (*t*1 − *t*0). Data is presented as mean and standard deviation of three independent experiments.

Acknowledgements

Notes and references

1 K. S. Novoselov, V. I. Fal'ko, L. Colombo, P. R. Gellert, M. G. Schwab and K. Kim, *Nature*, 2012, **490**, 192–200.
2 A. C. Ferrari, F. Bonaccorso, V. Fal'ko, K. S. Novoselov, S. Roche, P. Boggild, S. Borini, F. H. Koppens, V. Palermo, N. Pugno, J. A. Garrido, R. Sordan, A. Bianco, L. Ballerini, M. Prato, E. Lidorikis, J. Kivioja, C. Marinelli, T. Ryhanen, A. Morpurgo, J. N. Coleman, V. Nicolosi, L. Colombo, A. Fert, M. Garcia-Hernandez, A. Bachtold, G. F. Schneider, F. Guinea, C. Dekker, M. Barbone, Z. Sun, C. Galiotis, A. N. Grigorenko, G. Konstantatos, A. Kis, M. Katsnelson, L. Vandersypen, A. Loiseau, V. Morandi, D. Neumaier, E. Treossi, V. Pellegrini, M. Polini, A. Tredicucci, G. M. Williams, B. H. Hong, J. H. Ahn, J. M. Kim, H. Zirath, B. J. van Wees, H. van der Zant, L. Occhipinti, A. Di Matteo, I. A. Kinloch, T. Seyller, E. Quesnel, X. Feng, K. Teo, N. Rupesinghe, P. Hakonen, S. R. Neil, Q. Tannock, T. Lofwander and J. Kinaret, *Nanoscale*, 2015, **7**, 4598–4810.
3 W. S. Hummers and R. E. Offeman, *J. Am. Chem. Soc.*, 1958, **80**, 1339.
4 K. S. Novoselov, A. K. Geim, S. V. Morozov, D. Jiang, Y. Zhang, S. V. Dubonos, I. V. Grigorieva and A. A. Firsov, *Science*, 2004, **306**, 666–669.
5 Y. Hernandez, V. Nicolosi, M. Lotya, F. M. Blighe, Z. Sun, S. De, I. T. McGovern, B. Holland, M. Byrne, Y. K. Gun'Ko, J. J. Boland, P. Niraj, G. Duesberg, S. Krishnamurthy, R. Goodhue, J. Hutchison, V. Scardaci, A. C. Ferrari and J. N. Coleman, *Nat. Nanotechnol.*, 2008, **3**, 563–568.

6 V. Leon, M. Quintana, M. A. Herrero, J. L. Fierro, A. de la Hoz, M. Prato and E. Vazquez, *Chem. Commun.*, 2011, **47**, 10936–10938.

7 J. Cai, P. Ruffieux, R. Jaafar, M. Bieri, T. Braun, S. Blankenburg, M. Muoth, A. P. Seitsonen, M. Saleh, X. Feng, K. Mullen and R. Fasel, *Nature*, 2010, **466**, 470–473.

8 J. Liu, B. W. Li, Y. Z. Tan, A. Giannakopoulos, C. Sanchez-Sanchez, D. Beljonne, P. Ruffieux, R. Fasel, X. Feng and K. Mullen, *J. Am. Chem. Soc.*, 2015, **137**, 6097–6103.

9 M. G. Schwab, A. Narita, S. Osella, Y. Hu, A. Maghsoumi, A. Mavrinsky, W. Pisula, C. Castiglioni, M. Tommasini, D. Beljonne, X. Feng and K. Mullen, *Chem. – Asian J.*, 2015, **10**, 2134–2138.

10 S. Stankovich, D. A. Dikin, R. D. Piner, K. A. Kohlhaas, A. Kleinhammes, Y. Jia, Y. Wu, S. T. Nguyen and R. S. Ruoff, *Carbon*, 2007, **45**, 1558–1565.

11 M. Inagaki and F. Kang, *J. Mater. Chem. A*, 2014, **2**, 13193–13206.

12 D. V. Kosynkin, A. L. Higginbotham, A. Sinitskii, J. R. Lomeda, A. Dimiev, B. K. Price and J. M. Tour, *Nature*, 2009, **458**, 872–876.

13 D. Bitounis, H. Ali-Boucetta, B. H. Hong, D.-H. Min and K. Kostarelos, *Adv. Mater.*, 2013, **25**, 2258–2268.

14 K. Kostarelos and K. S. Novoselov, *Nat. Nanotechnol.*, 2014, **9**, 744–745.

15 Z. Liu, J. T. Robinson, X. Sun and H. Dai, *J. Am. Chem. Soc.*, 2008, **130**, 10876–10877.

16 M. Melucci, M. Durso, M. Zambianchi, E. Treossi, Z.-Y. Xia, I. Manet, G. Giambastiani, L. Ortolani, V. Morandi, F. De Angelis and V. Palermo, *J. Mater. Chem.*, 2012, **22**, 18237.

17 S. Makharza, G. Cirillo, A. Bachmatiuk, I. Ibrahim, N. Ioannides, B. Trzebicka, S. Hampel and M. H. Rümmeli, *J. Nanopart. Res.*, 2013, 15.

18 G. Sechi, D. Bedognetti, F. Sgarrella, L. Van Eperen, F. M. Marincola, A. Bianco and L. G. Delogu, *Nanomedicine*, 2014, **9**, 1475–1486.

19 A. Bianco, *Angew. Chem. Int. Ed.*, 2013, **52**, 4986–4997.

20 A. Bianco, H.-M. Cheng, T. Enoki, Y. Gogotsi, R. H. Hurt, N. Koratkar, T. Kyotani, M. Monthioux, C. R. Park, J. M. D. Tascon and J. Zhang, *Carbon*, 2013, **65**, 1–6.

21 P. Wick, A. E. Louw-Gaume, M. Kucki, H. F. Krug, K. Kostarelos, B. Fadeel, K. A. Dawson, A. Salvati, E. Vazquez, L. Ballerini, M. Tretiach, F. Benfenati, E. Flahaut, L. Gauthier, M. Prato and A. Bianco, *Angew. Chemie*, 2014, **53**, 7714–7718.

22 C. Bussy, D. Jasim, N. Lozano, D. Terry and K. Kostarelos, *Nanoscale*, 2015, **7**, 6432–6435.

23 L. Ma-Hock, V. Strauss, S. Treumann, K. Kuttler, W. Wohlleben, T. Hofmann, S. Groters, K. Wiench, B. van Ravenzwaay and R. Landsiedel, *Part. Fibre Toxicol.*, 2013, **10**, 23.

24 A. Schinwald, F. Murphy, A. Askounis, V. Koutsos, K. Sefiane, K. Donaldson and C. J. Campbell, *Nanotoxicology*, 2014, **8**, 824–832.

25 L. De Marzi, L. Ottaviano, F. Perrozzi, M. Nardone, S. Santucci, J. De Lapuente, M. Borras, E. Treossi, V. Palermo and A. Poma, *J. Biol. Regul. Homeostatic Agents*, 2014, **28**, 281–289.

26 K. Kouroupis-Agalou, A. Liscio, E. Treossi, L. Ortolani, V. Morandi, N. M. Pugno and V. Palermo, *Nanoscale*, 2014, **6**, 5926–5933.

27 A. A. Green and M. C. Hersam, *Nano Lett.*, 2009, **9**, 4031–4036.

28 M. Lotya, P. J. King, U. Khan, S. De and J. N. Coleman, *ACS Nano*, 2010, **4**, 3155–3162.

29 A. Liscio, K. Kouroupis-Agalou, X. Díez-Betriu, A. Kovtun, E. Treossi, N. M. Pugno, G. De Luca and V. Palermo, *Nature Commun.*, submitted.

30 R. Kurapati, J. Russier, M. A. Squillaci, E. Treossi, C. Ménard-Moyon, A. E. D. Rio-Castillo, E. Vazquez, P. Samorì, V. Palermo and A. Bianco, *Small*, 2015, **11**(32), 3985–3994.

31 D. Yang, A. Velamakanni, G. Bozoklu, S. Park, M. Stoller, R. D. Piner, S. Stankovich, I. Jung, D. A. Field, C. A. Ventrice and R. S. Ruoff, *Carbon*, 2009, **47**, 145–152.

32 S. Some, Y. Kim, E. Hwang, H. Yoo and H. Lee, *Chem. Commun.*, 2012, **48**, 7732–7734.

33 L. Stobinski, B. Lesiak, A. Malolepszy, M. Mazurkiewicz, B. Mierzwa, J. Zemek, P. Jiricek and I. Bieloshapka, *J. Electron Spectrosc. Relat. Phenom.*, 2014, **195**, 145–154.

34 L. G. Cancado, A. Jorio, E. H. Ferreira, F. Stavale, C. A. Achete, R. B. Capaz, M. V. Moutinho, A. Lombardo, T. S. Kulmala and A. C. Ferrari, *Nano Lett.*, 2011, **11**, 3190–3196.

35 J. Russier, E. Treossi, A. Scarsi, F. Perrozzi, H. Dumortier, L. Ottaviano, M. Meneghetti, V. Palermo and A. Bianco, *Nanoscale*, 2013, **5**, 11234–11247.

36 M. Roesslein, C. Hirsch, J. P. Kaiser, H. F. Krug and P. Wick, *Int. J. Mol. Sci.*, 2013, **14**, 24320–24337.

37 A. Bachmatiuk, R. G. Mendes, C. Hirsch, C. Jähne, M. R. Lohe, J. Grothe, S. Kaskel, L. Fu, R. Klingeler, J. Eckert, P. Wick and M. H. Rümmeli, *ACS Nano*, 2013, **7**, 10552–10562.

38 A. Jos, S. Pichardo, M. Puerto, E. Sanchez, A. Grilo and A. M. Camean, *Toxicol. in Vitro*, 2009, **23**, 1491–1496.

39 Y. Chang, S. T. Yang, J. H. Liu, E. Dong, Y. Wang, A. Cao, Y. Liu and H. Wang, *Toxicol. Lett.*, 2011, **200**, 201–210.

40 E. Treossi, M. Melucci, A. Liscio, M. Gazzano, P. Samori and V. Palermo, *J. Am. Chem. Soc.*, 2009, **131**, 15576–15577.

41 J. F. Moulder, W. F. Stickle, P. E. Sobol and K. D. Bomben, *Handbook of X-ray Photoelectron Spectroscopy*, Physical Electronics Inc., Eden Prairie, MN, USA, 1995.